

Voltage-controllable multiwavelength InAs quantum-dot infrared photodetectors for mid- and far-infrared detection

Zhengmao Ye^{a)} and Joe C. Campbell^{b)}

Microelectronics Research Center, University of Texas at Austin, 10,100 Burnet Road, Bldg. 160, Austin, Texas 78712-1100

Zhonghui Chen, Eui-Tae Kim, and Anupam Madhukar

Departments of Materials Science and Physics, University of Southern California, Los Angeles, California 90089

(Received 31 January 2002; accepted for publication 10 July 2002)

We report a bias-controllable multiwavelength quantum dot infrared photodetector (QDIP). The active region of the QDIP consisted of five layers of InAs quantum dots with InGaAs cap layers. Photoresponse peaks at 5.5, 5.9, 8.9, and 10.3–10.9 μm were observed. The relative response of these peaks could be controlled through the applied bias. For 5.9 μm detection, a peak detectivity, D^* , of $5.8 \times 10^9 \text{ cm Hz}^{1/2}/\text{W}$ at 77 K and 0.3 V was achieved. © 2002 American Institute of Physics. [DOI: 10.1063/1.1504167]

The quantum dot infrared photodetectors (QDIPs) have recently been the subject of numerous research efforts,^{1–8} owing to their potential for high responsivity and low dark current in the midwavelength infrared (MWIR) and long-wavelength infrared (LWIR) spectral regions. By controlling quantum dot (QD) size, and the characteristics of the barrier potential, QDIPs with a single photoresponse peak in the wavelength range from 3.5 to 13 μm have been reported.^{2–8} QDIPs with bias-controllable spectral response are attractive for multiwavelength applications such as temperature registration, solid-state spectrometers, target discrimination and identification, and chemical analysis. Previously, two- or three-color quantum well infrared photodetectors (QWIPs) for mid, long, and very long infrared detection have been reported. These QWIPs showed the peak detectivities of 2.96×10^{10} ($\lambda=9 \mu\text{m}$), 8.7×10^{10} ($\lambda=7.4 \mu\text{m}$), 8.5×10^{12} ($\lambda=6.5 \mu\text{m}$), and $2.2 \times 10^{12} \text{ cm Hz}^{1/2}/\text{W}$ ($\lambda=7.4 \mu\text{m}$) at 77, 70, 40, and 5 K, respectively.^{9–12} QDIPs have the potential for higher photoresponse to infrared radiation and higher temperature operation than QWIPs, as a result of the long carrier capture and relaxation times in QDIPs. Most importantly, the three-dimensional confinement of electrons in the QD permits QDIPs to operate in the normal incidence mode, unlike n -type QWIPs which are not sensitive to radiation that is incident perpendicular to the quantum wells.¹ Recently, we reported a bias-controllable dual-wavelength photoresponse^{13,14} in a QDIP structure that incorporated InAs QD layers with two different QD size distributions. In this article we report on the photodetector characteristics of this structure. Although only five layers of QD were used, owing to its low dark current, this QDIP achieved high detectivity compared with published detectivity for QDIPs.^{2–8}

The multiwavelength QDIP in this work was an n - i - n structure. The samples have the same structure as reported in Refs. 13 and 14. A cross-sectional transmission electron microscope dark-field image of the QD structure, along with an

atomic force microscopy study on uncapped InAs pyramidal-shaped QDs, show that QDs in the first three layers had an average height of 56 Å and dot density of $\sim 4 \times 10^{10}/\text{cm}^2$, while the QDs in the fifth layers show an average height of 30 Å and dot density of $\sim 1 \times 10^{10}/\text{cm}^2$. The bimodal distribution of the QDs underlies the reported^{13,14} dual wavelength photoresponse and suggests the potential for two-color operation of a QD photodetector.

Mesas having a diameter of 250 μm and a height of $\sim 1.4 \mu\text{m}$ were defined with an etch of $\text{H}_3\text{PO}_4:\text{H}_2\text{O}_2:\text{H}_2\text{O}$ (8:1:1). A 50 μm diameter top contact and the bottom contact were formed by evaporation and lift-off of Au/Ni/AuGe. The contacts were then annealed at 430 °C for 20 s. In the following discussion, “positive” bias means that a positive voltage was applied to the top contacts.

The normal-incidence photoresponse was measured with a Nicolet Magna-IR 570 Fourier-transform infrared (FTIR) spectrometer and a SRS 570 low-noise current preamplifier. In order to rule out parallel propagation of light reflected from the mesa sidewall, we measured the spectral response of the QDIPs with metal defined opening on the top of the mesa, whose diameter (220 μm) was smaller than that of the mesa (250 μm). By using this metal cover, the parallel propagating light reflected off from the detector mesa sidewall was negligible. The sidewall of the sample was also covered with opaque material. The spectral response demonstrated no significant change of the peak wavelength and the magnitude of the photocurrent, which suggested that the photocurrent arising from the light reflected off from the mesa sidewall did not significantly affect the photoresponse and the QDIP photocurrent arises from normally-incident radiation. Figure 1 shows the bias dependence of the photoresponse spectra at 77 K. At negative bias, the sample exhibits two main intraband photoresponse peaks, one at 5.5 μm and the other at 8.9 μm with full width at half maximum of ~ 0.7 and 1.0 μm , respectively. For both peaks, $\Delta\lambda/\lambda \approx 12\%$. The narrow spectral width suggests that the electron transitions are intraband bound to bound. The nature of the final states involved is discussed in Refs. 14 and 15. Broadening of the

^{a)}Electronic mail: zmye@mail.utexas.edu

^{b)}Electronic mail: jcc@mail.utexas.edu

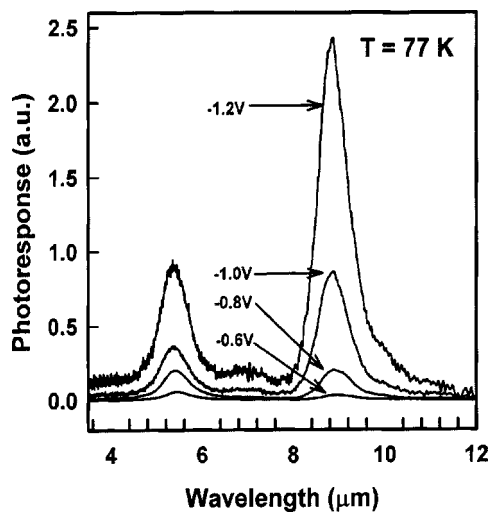


FIG. 1. Normal-incident photoresponse of the QDIP at 77 K. The photoresponses of both peaks increase with increasing bias.

spectral width results from the nonuniformity of the QDs size. The increase in the photoresponse with bias is due to the fact that as the bias increases, the lowering of the barrier at the contact layers causes more electrons to occupy the lower states of the QDs and participate in photon induced intraband transitions.

Figure 2 shows the spectral response and illustrates the bias-controllable multicolor characteristic. At low negative bias, the main photoresponse peak occurred at $5.5 \mu\text{m}$. This is due to the fact that the lower electron states in the larger QDs, whose intraband transitions contribute to the photoresponse of the $5.5 \mu\text{m}$ peak,^{13,14} are partially occupied; the small QDs, whose intraband transitions contribute to the photoresponse of the $8.9 \mu\text{m}$ peak,^{13–15} are relatively unoccupied. This results from the lower electron ground state energy (measured with respect to the GaAs conduction band edge) of larger QDs.^{13,14} With increasing bias, the dark current increases, which results in increasing occupation of the electron ground states of the small QDs. The photoresponse for the $8.9 \mu\text{m}$ peak is observed when the applied bias is greater than $\pm 0.2 \text{ V}$. We hypothesize that the gain of the photoexcited electrons from the small QDs increases more rapidly with bias than that of the large QDs.¹⁴ Therefore, the amplitude of the $8.9 \mu\text{m}$ peak increases much faster than that of the $5.5 \mu\text{m}$ peak. At $\sim -0.8 \text{ V}$, the peak amplitudes of the 5.5 and $8.9 \mu\text{m}$ peaks are comparable. With further increase in bias, the intraband photocurrent of the small QDs exceeds that of the large QDs. For a bias of -1.2 V , the $8.9 \mu\text{m}$ peak dominates. The multiwavelength characteristic is also observed for positive bias. Both peaks exhibited a redshift relative to the negative bias case. The spectral response of the shorter wavelength peak shifts to $5.9 \mu\text{m}$, while two peaks emerge in the $10.3\text{--}10.9 \mu\text{m}$ region. We attribute the asymmetric behavior for negative and positive bias to the asymmetric potential caused by the pyramidal QD shape and the InGaAs capping layer before. Therefore, electrons in the QDs experience different potential profiles when they travel toward the top contact or the bottom contact.

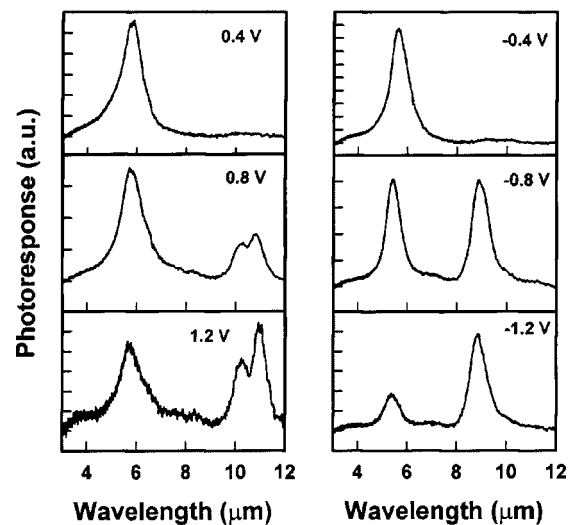


FIG. 2. Photoresponse at 0.4, 0.8, and 1.2 V; -0.4 , -0.8 , and -1.2 V .

The absolute spectral responsivity was calibrated with a blackbody source at the temperature of 700°C . For each peak, filters with different bandpass wavelength were used so that the responsivity of each peak was calibrated individually. Figure 3 shows the peak spectral responsivity versus bias at 77 K. With increase in bias, the responsivities of all four peaks increase four orders of magnitude from $\sim 10^{-4} \text{ A/W}$ at low bias to $\sim 1 \text{ A/W}$ at -1.3 V . For negative bias, the crossover of the responsivities of the two peaks occurs at $\sim -0.8 \text{ V}$, which is consistent with the FTIR measurement. The asymmetric responsivity curves for the positive and negative bias results from the asymmetric band structure that gives rise to the redshift of the photoresponse at positive bias.

Figure 4 shows dark I - V characteristics for the sample in a cold shield with temperature ranging from 20 to 296 K. The background-limited performance temperature, which refers to the temperature at which the current from the thermal background radiation is equal to the dark current, is also shown in the figure. At 77 K, the dark current density is $1.3 \times 10^{-6} \text{ A/cm}^2$ and $4.4 \times 10^{-3} \text{ A/cm}^2$ at -0.3 and -0.8 V , respectively. With increasing temperature from 40 K to room temperature, the dark current density increases over seven orders of magnitude. At low bias and $T > 77 \text{ K}$, the dark current increases exponentially by 10^6 with increasing temperature, which suggests that in this temperature range the dark current originates from thermionic emission. For temperature lower than 77 K, sequential resonant tunneling and phonon assisted tunneling are probably the dominant components of the dark current. Asymmetric dark current density for positive and negative bias is observed, which is also caused by the asymmetry of the band structure.

The thermal noise current can be expressed as, $I_{\text{th}} = \sqrt{4kT/R}$, where k is Boltzmann's constant, T is the absolute temperature, and R is the differential resistance of the device, which is calculated from the dark current measurement. At $V_B = \pm 0.3 \text{ V}$, the calculated thermal noise current ($1.1 \times 10^{-14} \text{ A/Hz}^{1/2}$) is very close to the measured noise current ($1.3 \times 10^{-14} \text{ A/Hz}^{1/2}$), which indicates that thermal noise is significant in the low bias region (Fig. 5). As the bias

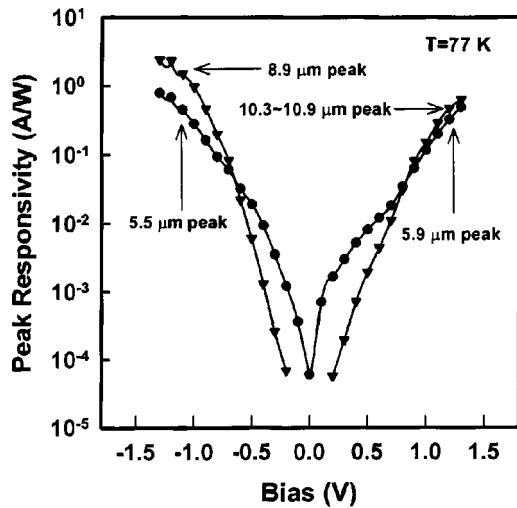


FIG. 3. Peak responsivity of each peak at 77 K.

increases, the noise current increases much faster than thermal noise and the shot noise becomes dominant at higher bias.

The responsivity and noise current were used to estimate the detectivity at 77 K using the relation $D^* = R\sqrt{A\Delta f}/i_n$, where A is the device area, R is the responsivity, i_n is the noise current, and Δf is the bandwidth. For the shorter wavelength peaks, the QDIP had the best performance at 0.3 V with a peak detectivity of $5.8 \times 10^9 \text{ cm Hz}^{1/2}/\text{W}$ for the 5.9 μm peak, and at -0.3 V with a peak detectivity of $3.7 \times 10^9 \text{ cm Hz}^{1/2}/\text{W}$ for the 5.5 μm peak. The corresponding responsivities were 3.5 and 3.0 mA/W, respectively. For the longer wavelength peaks, the QDIP had the best performance at -0.8 V with a peak detectivity of $7.3 \times 10^8 \text{ cm Hz}^{1/2}/\text{W}$ for the 8.9 μm peak, and at 0.5 V with a peak detectivity of $7.3 \times 10^8 \text{ cm Hz}^{1/2}/\text{W}$ for the 10.3–10.9 μm peaks. The corresponding responsivities were 200 and 1.9 mA/W, respectively. The relatively lower detectivities for the longer wavelength peaks reflect the rapid increase in noise with

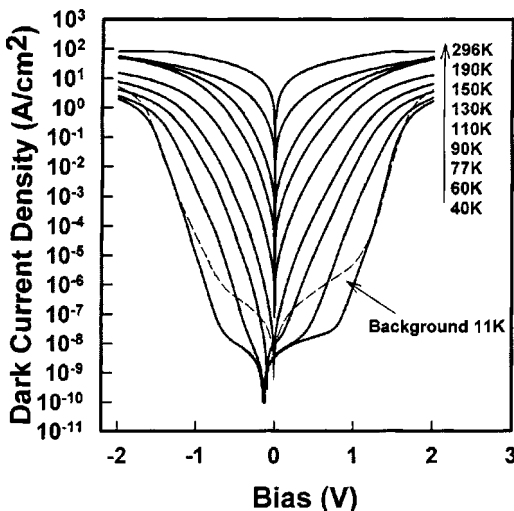


FIG. 4. Dark current density vs voltage for temperature in the range 20–296 K.

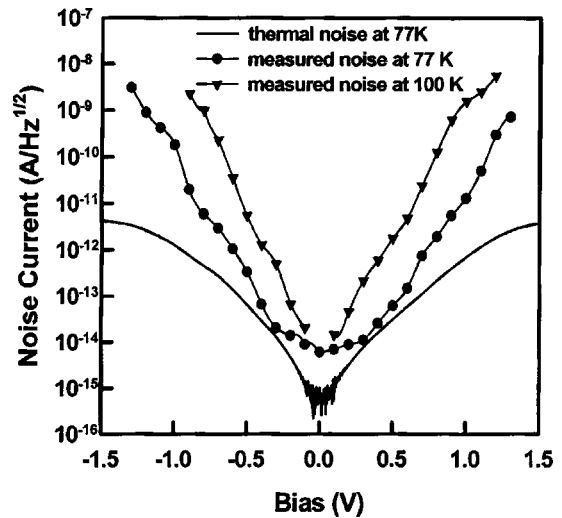


FIG. 5. Measured noise current and calculated thermal noise current at 77 K.

increasing bias. The detectivity of the two-color QDIP is still lower than that of multiwavelength QWIPs, which is mainly due to the lower responsivity as a result of the lower dot density and fewer quantum dot layers. QDIPs with more active layers may achieve higher responsivity if dot size and density can be maintained.

In conclusion, we have demonstrated a bound-to-bound InAs/InGaAs QDIP with multiwavelength response. By tuning the applied bias, the QDIP exhibited operation with photoresponse MWIR peaks centered at 5.5 and 5.9 μm , and LWIR response at 8.8 and 10.3–10.9 μm . Low dark current and noise current were achieved. The highest detectivity was $D^* = 5.8 \times 10^9 \text{ cm Hz}^{1/2}/\text{W}$ and $R = 3.5 \text{ mA/W}$ at 0.3 V bias and 77 K for the 5.9 μm photoresponse peak.

This work was supported by AFOSR under the MURI program.

- ¹V. Ryzhii, *Sci. Technol.* **11**, 759 (1996).
- ²D. Pan, E. Towe, and S. Kennerly, *Appl. Phys. Lett.* **75**, 2719 (1999).
- ³S. Kim, H. Mohseni, M. Erdtmann, E. Michel, C. Jelen, and M. Razeghi, *Appl. Phys. Lett.* **73**, 963 (1998).
- ⁴A. Stiff, S. Krishna, P. Bhattacharya, and S. W. Kennerly, *IEEE J. Quantum Electron.* **37**, 1412 (2001).
- ⁵Z. Chen, O. Baklenov, E. T. Kim, I. Mukhametzhanov, J. Tie, A. Madhukar, Z. Ye, and J. C. Campbell, *J. Appl. Phys.* **89**, 4558 (2001).
- ⁶S. Y. Lin, Y. R. Tsai, and S. C. Lee, *Appl. Phys. Lett.* **78**, 2784 (2001).
- ⁷J. W. Kim, J. E. Oh, S. C. Hong, C. H. Park, and T. K. Yoo, *IEEE Electron Device Lett.* **21**, 329 (2000).
- ⁸S. Y. Wang, S. D. Lin, H. W. Wu, and C. P. Lee, *Appl. Phys. Lett.* **78**, 1023 (2001).
- ⁹A. Köck, E. Gornik, G. Abstreiter, G. Böhm, M. Walther, and G. Weimann, *Appl. Phys. Lett.* **60**, 2011 (1992).
- ¹⁰X. D. Jiang, S. S. Li, and M. Z. Tidrow, *IEEE J. Quantum Electron.* **35**, 1685 (1999).
- ¹¹C. C. Chen, H. C. Chen, C. H. Kuan, S. D. Lin, and C. P. Lee, *Appl. Phys. Lett.* **80**, 2251 (2002).
- ¹²L. Jiang, S. S. Li, M. Z. Tidrow, W. R. Dyer, W. K. Wu, J. M. Fastenau, and T. R. Yurasits, *Appl. Phys. Lett.* **79**, 2982 (2001).
- ¹³E. T. Kim, Z. H. Chen, M. Ho, and A. Madhukar, *J. Vac. Sci. Technol.* (in press).
- ¹⁴Z. H. Chen, E. T. Kim, and A. Madhukar, *Appl. Phys. Lett.* **80**, 2490 (2002).
- ¹⁵E. T. Kim, Z. H. Chen, and A. Madhukar, *Appl. Phys. Lett.* **79**, 3341 (2001).